Microchim Acta (2017) 184:3909–3917
DOI 10.1007/s00604-017-2397-7

ORIGINAL PAPER

Ultrasensitive DNAzyme based amperometric determination of uranyl ion using mesoporous silica nanoparticles loaded with Methylene Blue

Yi Wen[1] · Yali Yuan[1] · Le Li[2] · Dandan Ma[3] · Qi Liao[1] · Shaoyan Hou[1]

Received: 14 March 2017 / Accepted: 26 June 2017 / Published online: 21 July 2017

Abstract The authors describe an ultrasensitive amperometric enzymatic assay for uranyl ion. It is based on the use of mesoporous silica nanoparticles (mesoSiNPs) loaded with Methylene Blue (MB) and functionalized with an UO_2(II)-dependent DNAzyme. The electroactive label MB was sealed in the inner pores of the mesoSiNPs along with double stranded DNA (containing the DNAzyme and the substrate strand). In the presence of UO_2(II), the DNAzyme is actived to cleave the substrate strands. This leads to the cleavage of the caps and the release of MB from the mesoSiNPs. The amount of released MB depends on the concentration of UO_2(II) and can be determined amperometrically, best at a working voltage of −0.25 V (vs SCE), by using a chitosan coated carbon paste electrode. Response is linear in the 20 pM to 0.1 nM UO_2(II) concentration range, and the detection limit is as low as 0.15 pM. Recoveries from spiked samples varied from 91.3 to 99.4%. The assay is highly specific, selective, and not interfered by other metal ions.

Keywords Mesoporous silica nanoparticles · DNAzymes · Amperometry · Electrochemical biosensor

Introduction

Uranium is a radioactive metal that is widely used in nuclear weapons, nuclear power plants, and so on [1]. Since uranium is one of the main sources in nuclear energy generation, it can be released into the environment and groundwater via uranium mining and improper disposal of nuclear waste [2]. Uranium exists in a variety of chemical forms in nature, while uranyl ion (UO_2^{2+}) is the most stable chemical species in aqueous solution that represents the greatest risk to human beings and other living species because of its bioavailability [3]. Therefore, it's imperative that the development of novel UO_2^{2+} detection methods that are efficient, sensitive and selective and applicable to aqueous systems. So far, various instrumental techniques, for example, spectroscopic analysis [4], mass spectrometry [5], atomic absorption spectroscopy [6], cold vapor atomic fluorescence spectrometry [7] were developed for the detection of UO_2^{2+} in aqueous solution. However, these techniques need expensive instruments, and moreover, the sample preparation is time-consuming and tedious.

To reduce instrumentation costs and time of sample preparation, the methods of detection of UO_2^{2+} have been reported. For example, *Kumar* et al. reported a simple analytical method for detection of UO_2^{2+} via photoluminescence quenching of amino-modified cadmium sulfide quantum dots [8]. In addition, *Khashab* et al. presented an efficient colorimetric peroxidase mimetic method to detect UO_2^{2+} by BSA-stabilized gold nanoclusters (BSA-AuNCs). In the absence of UO_2^{2+}, the BSA-AuNCs showed an instrnsic peroxidase like activity [9]. In the presence of UO_2^{2+}, this activity can be efficiently

Electronic supplementary material The online version of this article (doi:10.1007/s00604-017-2397-7) contains supplementary material, which is available to authorized users.

✉ Yali Yuan
yuanyali6439@163.com

[1] School of Chemistry and Chemical Engineering, University of South China, Hengyang 421001, Hunan, People's Republic of China

[2] School of Public Health, University of SouthNanhua, Hengyang 421001, Hunan, People's Republic of China

[3] State Key Laboratory of Chemo/Biosensing and Chemometrics, College of Chemistry and Chemical Engineering, Hunan University, Changsha 410082, China

restrained. However, these methods have relatively poor selectivity, which do not meet the requirement of rapid detection of UO_2^{2+} in aqueous environment. Deoxyribozymes (DNAzymes) which are DNA molecules with high specificity for a number of metal ions have attracted more attention [10–13]. So far, a number of highly specific DNAzymes have been isolated and used for detecting metal ions such as Pb^{2+}, Zn^{2+}, Cu^{2+}, Mn^{2+} and so on. Not long ago, a UO_2^{2+}-specific DNAzyme was reported by Lu and his coworkers. Encouraged by the discovery of UO_2^{2+}-specific DNAzyme, some DNAzyme based biosensors have been developed for the rapid and specific detection of UO_2^{2+}. For example, Lu and his coworkers have prepared a efficient colorimetric sensor for detection of UO_2^{2+} based on gold nanoparticles (AuNPs) and UO_2^{2+}-specific DNAzymes [14]. A fluorescent biosensor for detecting UO_2^{2+} was also developed based on UO_2^{2+}-specific DNAzymes and the fluorescence quenching ability of molybdenum disulfide (MoS_2) nanosheets [15]. Although some progress has been made over the past few years, it still is a significant challenge to design efficient and portable sensors for UO_2^{2+} detection with both high sensitivity and selectivity.

Among these techniques, electrochemical approaches have attracted more attention for good recognition capability, high sensitivity and selectivity, fast response and real time detection nature [16, 17]. Although our group prepared UO_2^{2+}-specific DNAzymes electrochemical biosensors for detection of UO_2^{2+} [18, 19], these methods have an intrinsic limitation in sensitivity, as one UO_2^{2+} converts only one signal readout. To achieve signal amplification and highly sensitive detection of UO_2^{2+}, mesoporous silica nanoparticles (mesoSiNPs) as carrier vehicles in this work, which has unique pore structure, biocompatibility, and ease of functionalization. More importantly, the large pore volume and surface area of mesoSiNPs make it possible to load large numbers of electroactive molecules.

In this system, we designed a novel electronic switch for detection of UO_2^{2+} by using MB-loaded and UO_2^{2+}-specific DNAzyme induced mesoSiNPs. In the presence of UO_2^{2+}, the release of more MB by the DNA substrate strand disrupting amplifies the electrochemical signal. The strategy establishes a efficient, high specificity and high sensitivity method for the detection of uranium, and provides a novel protocol for point-of-care testing of other metal ions.

Experimental

Chemicals and instruments

All DNA oligonucleotides used in this paper were designed according to articles and synthesized by Sangon Biotech Co., Ltd. (shanghai, China, http://www.sangon.com/), including the sequences (from 3′ to 5′) as described in Table S1 (in the Supporting Information) [14]. Cetyltrimethylammonium-bromide (CTAB), Sulfosuccinimidyl-4-(N-maleimidomethyl)-cyclohex -ane-1-carboxylate (Sulfo-SMCC), Tetraethylorthosilicate (TEOS), 3-aminopropyltriethoxysilane (APTES), Tris (hydroxymethyl) metyl aminomethane (Tris), Graphite powder, Paraffin oil, chitosan (chit) and Tris (2-carboxyethyl) phosphine hydrochloride (TCEP) were purchased from Aladdin Reagent Corporation (Shanghai, China, http://www.aladdin-e.com/). All other chemicals were of analytical grade, and were used without further purification. All aqueous solutions were prepared with ultrapure water (18.2 MΩ·cm, Milli-Q, Millipore). DNA hybridization buffer (pH 7.4) contained 10 mM Tris-HCl, 1 mM ethylenediaminetetraacetic acid (EDTA). Phosphate -buffered saline (PBS, pH 7.4) contained 1.98 mM KH_2PO_4, 4.0 mM Na_2HPO_4, 2.6 mM KCl, 40 mM NaCl. Uranium nitrate hexahydrate was dissolved in water to make a 1 mM stock solution.

Electrochemical measurements were performed on a CHI660C electrochemical workstation (CH Instruments, Chenhua Co., Ltd. China, http://www.chinstr.com/). A conventional three-electrode cell assembly consisting of a modified carbon paste electrode (CPE) (3.5 mm in diameter) serving as the working electrode, a KCl saturated calomel electrode as the reference electrode and platinum (Pt) wire as the counter electrode. All measurements were carried out at room temperature. The scanning electron microscope (SEM) images were obtained with a JSM-6700F instrument (JEOL Ltd., Japan, http://www.jeol.co.jp/cn/). Zeta-potential analysis was performed on a Zetasizer (Nano-Z, Malvern, UK, http://www.chem17.com/st15315/product_ 139,196.html). Nitrogen absorption/desorptionmeasurement was obtained with a Autosorb IQ (Quantachrome Instruments U.S., http://www.quantachrome-china.com).

Preparation and functionalization of the MesoSiNPs

In this research, according to the related articles, mesoSiNPs was prepared by sol-gel methods [20]. Briefly, cetyltrimethylammonium bromide (CTAB, 1.8 g) was dissolved in double distilled water (864 mL), followed by addition of NaOH (2 M, 6.3 mL). The precipitation was stirred at 40 °C for 2 h and followed by adjusting the solution temperature to 80 °C. Next, the tetraethylorthosilicate (TEOS) (9 mL) was added dropwise to precipitate at a rate of 1 mL·min^{-1}. After stirring 2 h, the white SiO_2 precursor were washed and dried under vacuum at 100 °C for 12 h. Then it was transferred into a muffle furnace and slowly heated to 550 °C for 6 h. The obtained white powder was mesoSiNPs that removed the template phase.

Next, sample of the extracted mesoSiNPs (3 g) was refluxed in anhydrous ethanol (100 mL) with 3-

aminopropyltriethoxysilane (APTES) (3 mL) inside a round bottom flask and stirred at 60 °C in water bath. After 6 h of reaction time, the reaction mixture was filtered, washed with ethanol and then placed in a 100 °C vacuum drying ovens to obtain amino-mesoSiNPs (mesoSiNPs-AM).

Then, mesoSiNPs-AM (40 mg) was added to MB (0.26 mM, 40 mL) solution and the mixture was shaken at 220 r·min^{-1} and 40 °C for 1 h. The solid product was filtered, rinsed with water and dried to obtain MB-loaded mesoporous silica nanoparticle (mesoSiNPs-AM@MB) [21, 22].

Then, sulfosuccinimidyl-4-(N-maleimidomethyl)-cyclohexane-1-carboxylate (Sulfo-SMCC) (120 μL) was dissolved in PBS (10 mM, 1 mL), and reacted with mesoSiNPs-AM@MB (12 mg·mL^{-1}) for 30 min, and then precipitated by over desalting column and reacted with double-stranded DNA (dsDNA) for 30 min to immobilized the dsDNA onto the methylene blue-loaded silica nanomaterials and sealed the methylene blue in the pores of the silica (mesoSiNPs-AM@MB@dsDNA).

Fabrication of electrode

The bare CPE was prepared by mixing graphite powder (87 mg) and paraffin oil (21 μL) in an agate mortar. The paste was then tightly pressed into a polypropylene tube with an inner diameter of 3.5 mm. A copper wire was inserted into the carbon paste to provide the electrical contact. The surface of the bare CPE was smoothed on a weighing paper [23].

Chitosan (chit) (50 mg) was dissolved in acetic acid (1%) solution for 40 min, which was adjusted in six different pH varied from 5.0 to 7.5 with NaOH (2 M), respectively. The mixture of dropping the chit in different pH (10 μL) and mesoSiNPs-AM@MB@dsDNA (20 μL) were applied to CPE, natural dried. The coated process was carried out on a clean bench.

Electrochemical measurements

The modification process of the sensor was detected by cyclic voltammetry (CV), differential pulse voltammetry (DPV), and electrochemical impedance spectroscopy (EIS). The three electrode system, which KCl saturated calomel electrode as reference electrode, platinum electrode as auxiliary electrode and CPE as working electrode was used. CV and EIS measurements were performed in PBS containing $[Fe(CN)_6]^{3-/4-}$ (5 mM). CV was conducted at the potential range of −0.1 V to 0.6 V under a scan rate of 0.1 V·s^{-1}. EIS was performed at a frequency ranging from 0.1 Hz to 100 kHz with a amplitude of 5 mV. DPV was carried out in PBS (10 mM, pH 7.4) at the potential range of −0.6 V to 0.6 V under modulation amplitude of 50 mV and a pulse width of 0.2 s. All experiments were carried out at room temperature.

Results and discussion

Detection mechanism

The electrochemical strategy was mainly based on mesoSiNPs-AM@MB@dsDNA as the signal nanoprobe for UO_2^{2+} detection. As depicted in Scheme 1a, the specifically recognizing DNAzyme is immobilized on the aminated mesoporous silica and sealed MB in the mesopores. Sulfo-SMCC was heterobifunctional crosslinkers that contained N-hydroxysuccinimide (NHS) ester and maleimide groups. Its NHS esters reacted with primary mesoSiNPs-AM to form amide bonds, while maleimides reacted with the thiolated modified dsDNA to form stable thioether bonds, which made the dsDNA immobilized on the surface of MB-loaded amino-functionalization mesoSiNPs.

The general principle of UO_2^{2+}-special DNAzyme as a stimuli-responsive cap for the controlled release of the MB loaded mesoSiNPs-based electrochemical biosensor for the detection of UO_2^{2+} (Scheme 1b). The chit and mesoSiNPs-AM@MB@dsDNA mixed dropp were applied to the CPE, when the presence of UO_2^{2+} induced the cleavage of the DNA substrate strand at the rA aposition to form two fragments, which led to the release of MB entrapped in the mesoSiNPs. Resulting in a larger electrochemical signal, by monitoring the change of the electrochemical signal that increased the peak current, the concentration of UO_2^{2+} can be indirectly determined with high sensitivity.

Choice of materials

According to the relevant articles, we found that the materials that can be applied to this sensor are graphene, polyaniline, polypyrrole (PPY) and mesoSiNPs and so on. But the irreversibility of graphene agglomeration leads to the poor capacitance performance; polyaniline has excellent conductivity, but its disorder of short fibrous and spherical morphology lead to its poor cycle stability; PPy lacks cycle stability and processing performance. Compared with other materials, mesoSiNPs as carrier vehicles in this work has many advantages of large specific surface area, unique pore structure, biocompatibility, and ease of functionalization, So that they have wide application in the drug release and enzyme immobilizatio. The enzyme immobilization process of mesoSiNPs can be applied in the field of enzyme immobilization, So the material was chosed to as electrode material.

Characterization of synthesized and MB-loaded mesoSiNPs

The morphology of mesoSiNPs was characterized by SEM (Fig. 1), which showed spherical particles of the uniform mesoSiNPs with a diameter around 100 nm.

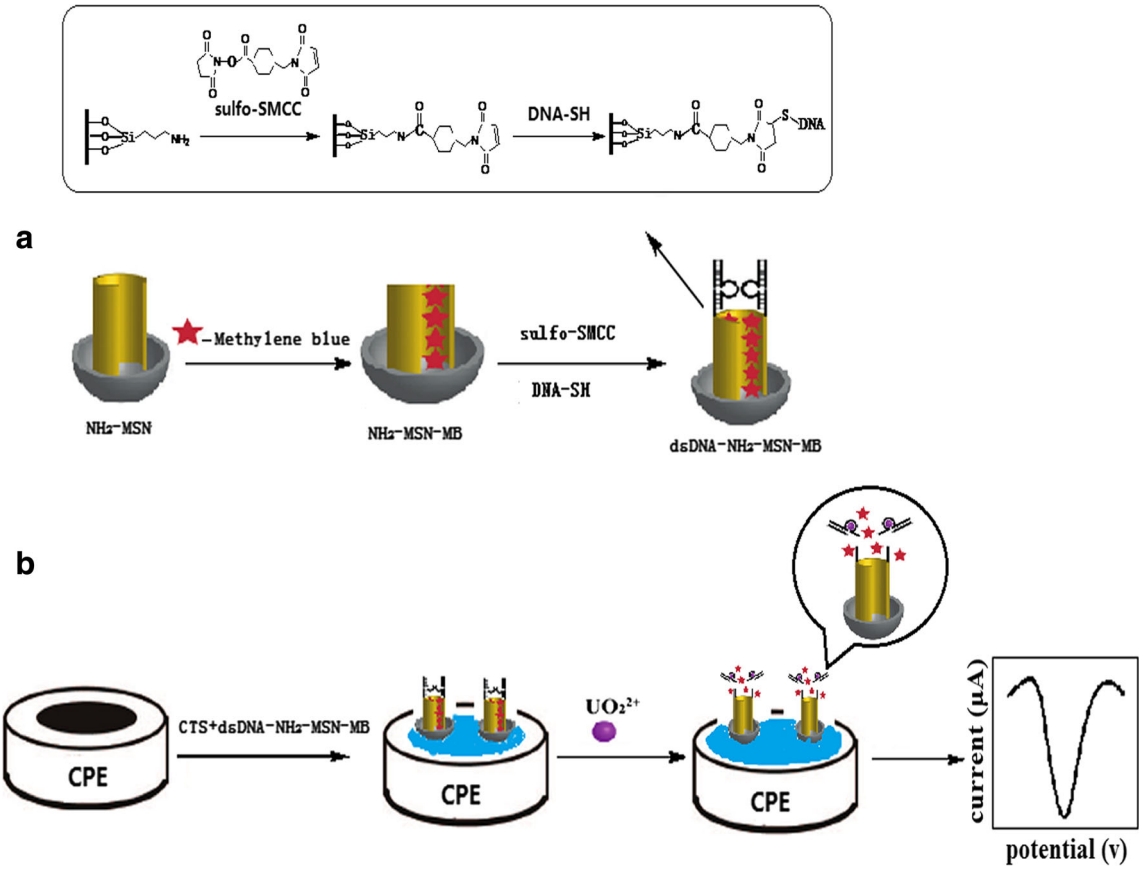

Scheme 1 **a** Schematic representation of the synthesis, MB loading, and dsDNA Binding of the mesoSiNPs, as well as the Release of MB from mesoSiNPs in the Presence of UO_2^{2+}. **b** Schematic Illustration of the Stepwise DNAzyme-based electrochemical sensor for uranium detection

The three mesoporous silica materials mesoSiNPs, mesoSiNPs-AM, mesoSiNPs-AM@MB and their precursors were analyzed by FT-IR, respectively (Fig. 2). The absorption peaks at 1228 cm^{-1} and 1093 cm^{-1} correspond to the asymmetric stretching vibration of Si-O-Si bond, and the absorption peaks at 787 cm^{-1} and 461 cm^{-1} belong to symmetry stretching of Si-O-Si bond Vibration and bending vibration, and the absorption peak at near 965 cm^{-1} attributes to Si-OH symmetrical stretching vibration. In Fig. 2a, the absorption peaks near 2930 cm^{-1} and 2847 cm^{-1} correspond to the stretching vibrations of CH_3 and CH_2 on the surfactant chain, respectively, and disappear completely in Fig. 2b. It is shown that by high temperature calcination, the template in the mesoporous material is effectively removed. As shown in Fig. 2c, a new vibration absorption peak at 1517 cm^{-1} is the deformation vibration of -NH_2 group, which indicates that the amino group had been successfully grafted onto the surface of the silica mesoporous material. The absorption peak of CH_3-N bond in MB is in the range of 2800–3500 cm^{-1}, corresponding to the absorption peak at 3280 cm^{-1} and 2899 cm^{-1} in Fig. 2d, and the peak at 1592 cm^{-1} from (d), the absorption peak at 1488 cm^{-1} is due to the stretching vibration of the C = C bond, which proved that MB has been successfully supported on the mesoSiNPs-AM.

Zeta-potential analysis is used to characterize the preparation of mesoSiNPs (Fig. S1a, in the Supporting Information). After APTES modification, the mesoSiNPs nanoparticles become positively charged, indicating that the amino groups are successfully functionalized on the surface of mesoSiNPs nanoparticles (Fig. S1b) [24, 25]. The loaded MB slightly increases the chargeability of

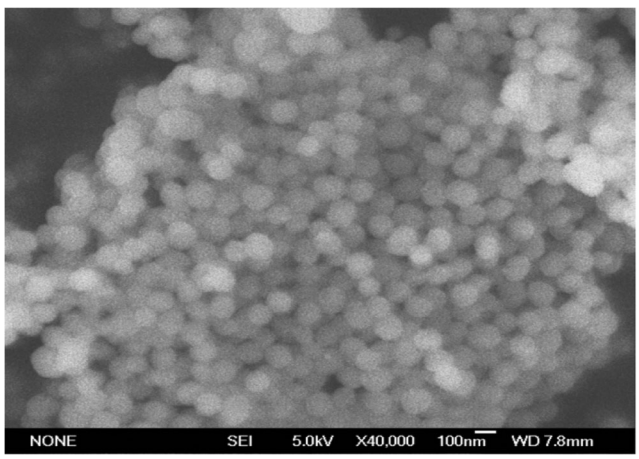

Fig. 1 SEM image of solid mesoSiNPs, showing the spherical morphology

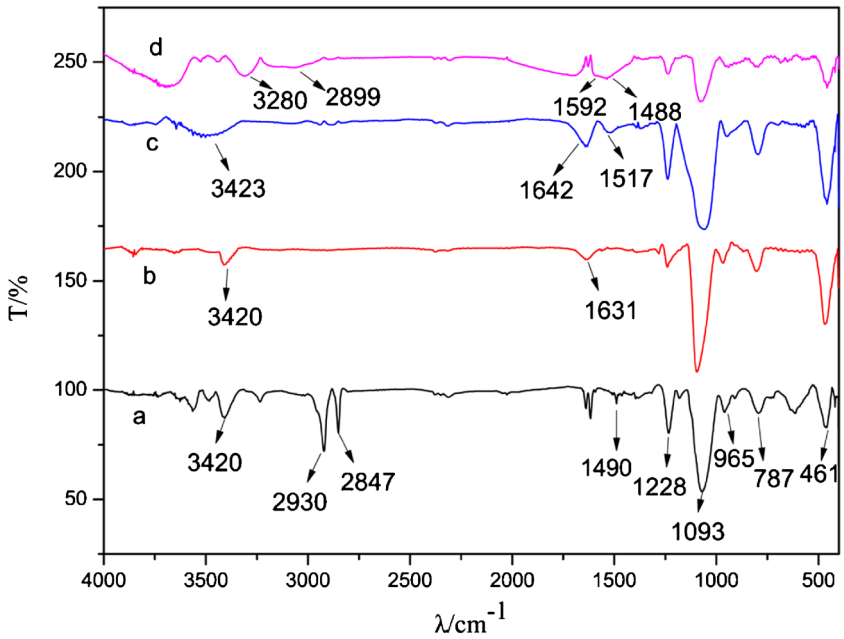

Fig. 2 FTIR spectra of (*a*) mesoSiNPs (Not removed the template), (*b*) mesoSiNPs, (*c*) mesoSiNPs-AM, (*d*) mesoSiNPs-AM@MB

the mesoSiNPs (Fig. S1c). The phosphate backbone of DNA covalently immobilize on the surface of mesoSiNPs making the methylene blue sealed in the inner pores that results in a negative charge of the mesoSiNPs (Fig. S1d). The experimental results are in agreement with the theory.

The nitrogen adsorption-desorption isotherm of the mesoSiNPs-AM showed an average pore diameter of 3.9 nm (Fig. 3). The total pore volume and total specific surface of mesoSiNPs-AM were calculated to be 0.71 $cm^3 \cdot g^{-1}$ and 796 $m^2 \cdot g^{-1}$ by using the BJH and BET model on the adsorption branch of the isotherm, respectively.

Optimization of sensor construction conditions

Before quantity analysis of UO_2^{2+} using this method, we optimised the sensor construction condition, including the DNA hybridization time, DNA concentration, pH on the chit, the different dosages of chit and mesoSiNPs-AM@MB@dsDNA, and the reaction time of the sensor with UO_2^{2+} on the system. As shown in Fig. S2–S4, the optimum values were 12 h hybridization time (Fig. S2), 80 μM DNA concentration (Fig. S3), chit pH 6.7 (Fig. S4), the chit and the MSN-AM@MB@dsDNA were mixed in the ratio of 1:2, and 20 min of reactived time of the sensor with UO_2^{2+} (Fig. S5) on the system (See the Supporting Information).

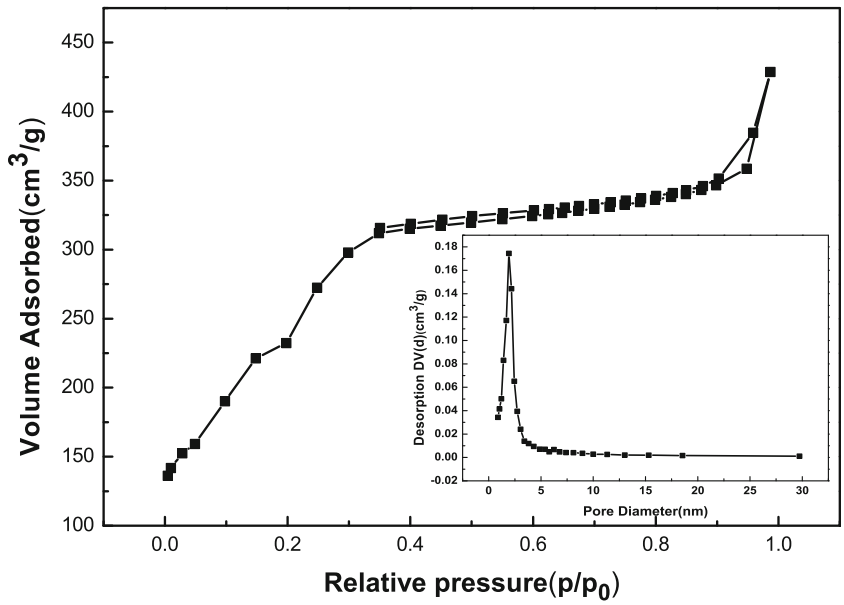

Fig. 3 Nitrogen adsorption-desorption isotherm of mesoSiNPs-AM. Inset: pore size distribution

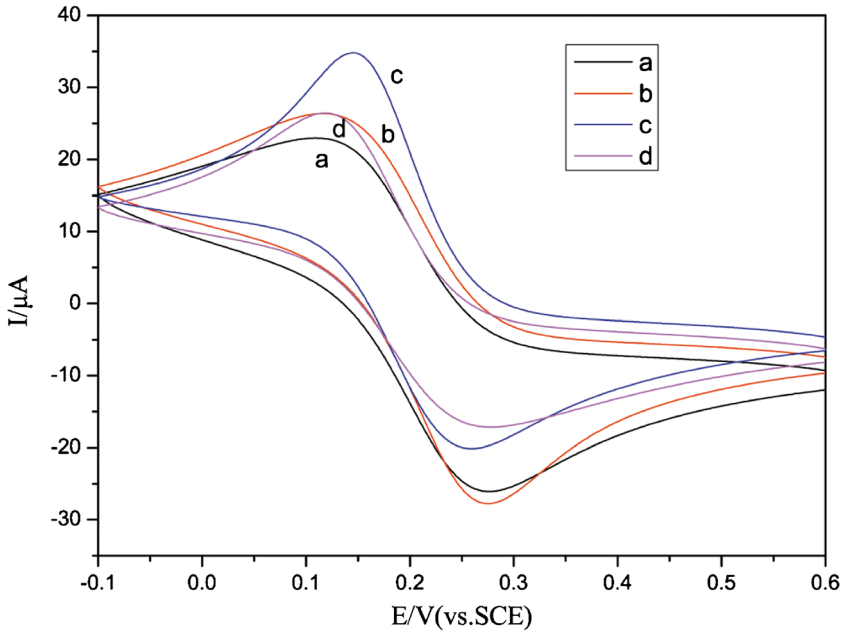

Fig. 4 CVs of different electrodes in PBS containing 5 mM $[Fe(CN)_6]^{3-/4-}$ at a scan rate of 100 $mV{\cdot}s^{-1}$ potential ranging from −0.1 V to 0.6 V. (*a*) bare CPE, (*b*) chit/CPE, (*c*) mesoSiNPs-AM@MB/chit/CPE, (*d*) mesoSiNPs-AM@MB@dsDNA/chit/CPE modified electrodes

Electrochemical characterization of different modified electrodes

The preparation process of the sensor was characterized by cyclic voltammetry (CV) and electrochemical impedance spectroscopy (EIS). CV was performed in PBS containing $[Fe(CN)_6]^{3-/4-}$ (5 mM) at a scan rate of 0.1 $V{\cdot}s^{-1}$ potential ranging from −0.1 V to 0.6 V, and the results were shown in Fig. 4.

As shown in Fig. 4, a pair of comparatively symmetrical redox peaks are observed at the bare carbon paste electrode (curve a), and the peak potential difference is 98 mV. After the chit is modified on the surface of the CPE, the peak current is increased due to the positive charge of chit, which makes the electrons easily reach the surface of the electrode (curve b). The increase of the peak current at the mesoSiNPs-AM@MB/chit/CPE (curve c) is due to the increase of the specific surface area and conductivity of the chit/CPE electrode, and with the addition of MB in the pores of the silica, the rate of surface diffusion of $[Fe(CN)_6]^{3-/4-}$ to the electrode becomes faster. When dsDNA is modified on the surface of mesoSiNPs-AM@MB/chit/CPE, the peak potential is reduced

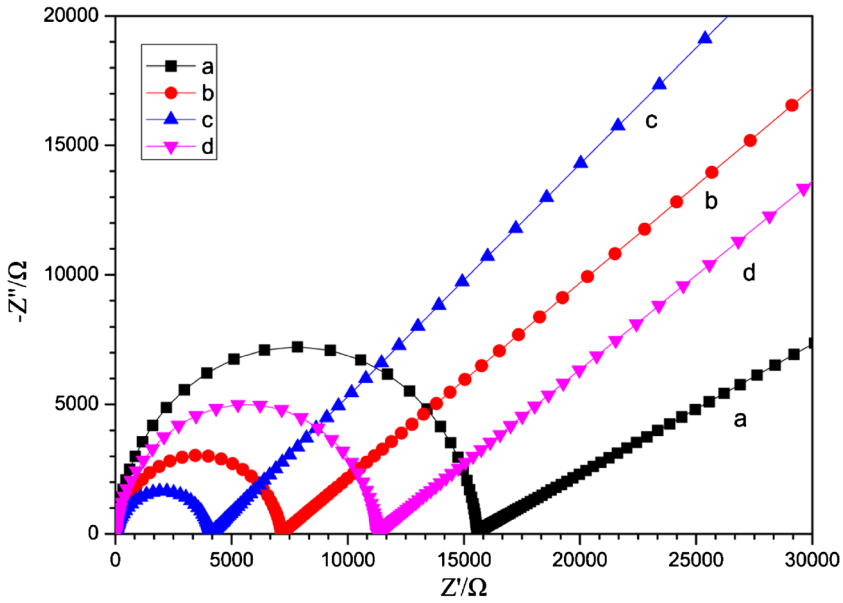

Fig. 5 Nyquist plots corresponding to (*a*) bare CPE, (*b*) chit/CPE, (*c*) mesoSiNPs-AM@MB/chit/CPE, (*d*) mesoSiNPs-AM@MB@dsDNA/chit/CPE electrodes in PBS (10 mmol/L, pH 7.4) containing 5 mM $[Fe(CN)_6]^{3-/4-}$ as the redox probe. The impedance spectra were recorded within the range from 100 kHz to 0.1 Hz at the formal potential of $[Fe(CN)6]^{3-/4-}$. The amplitude of the alternate voltage was 5 mV

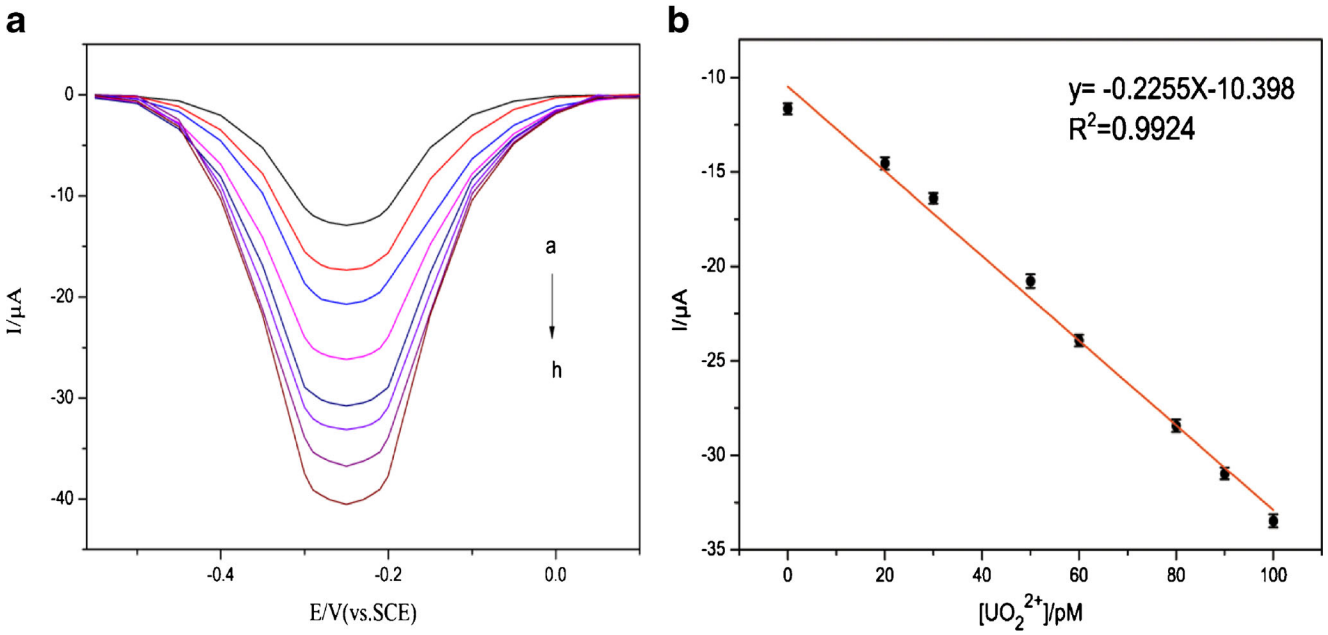

Fig. 6 **a** DPV curves of the electrode at different UO_2^{2+} concentration (*a*) no UO_2^{2+}, (*b*) 20 pM, (*c*) 30 pM, (*d*) 50 pM, (*e*) 60 pM, (*f*) 80 pM, (*g*) 90 pM, (h) 100 pM. **b** The peak current was linear with UO_2^{2+} concentration over the range of 20 pM to 100 pM

by 159 mV and the peak current decreases correspondingly, indicating that dsDNA have fully been enclosed the MB in the pores of mesoSiNPs, and dsDNA themselves negative charge repulsion $[Fe(CN)_6]^{3-/4-}$ leads to a slower electron transport rate (curve d).

EIS is also an effective method to characterize the surface properties of the modified electrode. The change of the semicircular diameter in the Nyquist spectrum can reflect the change of the surface property of the modified electrode.

As can be seen from Fig. 5, the semicircular diameter of the bare CPE is large, indicating that the electron transfer on the bare CPE is very slow. A dense membrane formed by modifying chit on the electrode surface increases the interface electron conduction rate and results in a lower impedance (Ret = 7.56 kΩ). After the mesoSiNPs-AM@MB is assembled on the chit-modified electrode, due to the nanomaterials increased the surface area of the electrode and the MB supported by the electroactive increased the conductivity of the electron, so the impedance is obviously decreased. When immobilized dsDNA onto the surface of the mesoSiNPs, the impedance increases from 7.56 kΩ to 11.4 kΩ, which proved that the dsDNA has sealed the MB in the pores of the mesoSiNPs successfully, the immobilized dsDNA prevented the diffusion of ferricyanide to the electrode surface. Based on the characterization of EIS and CV, it can be concluded that the modification process of the electrode reached the expected results.

Electrochemical detection of uranyl ion content

DPV detection was carried out in PBS containing different concentrations of UO_2^{2+} with mesoSiNPs-AM@MB@dsDNA/chit/CPE as the working electrode. As shown in Fig. 6a, the oxidation peak current of MB is increased with the increase of UO_2^{2+} concentrations.

The concentrations of UO_2^{2+} and the peak current at the concentration range of 20 pM to 100 pM show a good linear relationship (Fig. 6b). The linear equation is I/A = −10.398-0.2255 c/pM, (where I and c represent the peak current and UO_2^{2+} concentration, respectively.) The correlation coefficient is 0.9924 and the detection limit is estimated to be 0.15 pM based on 3 S/m, here S is the standard deviation of the intercept and m is the slope of the regression line [26]. This sensor is more effective than other reported uranium-based sensors (Table 1).

Table 1 Performance of different uranium sensors

Method	Technique	LOD	Linear range	Reference
Electrochemical	(DPV)	0.15 pM	20 pM-0.1 nM	This work
Electrochemical	(DPV)	2 pM	10 pM-1 nM	[27]
Electrochemical	(DPV)	12 pM	22 pM-0.13 nM	[18]
Resonance light scattering	(RLS)	6.7 nM	22 nM–550 nM	[28]

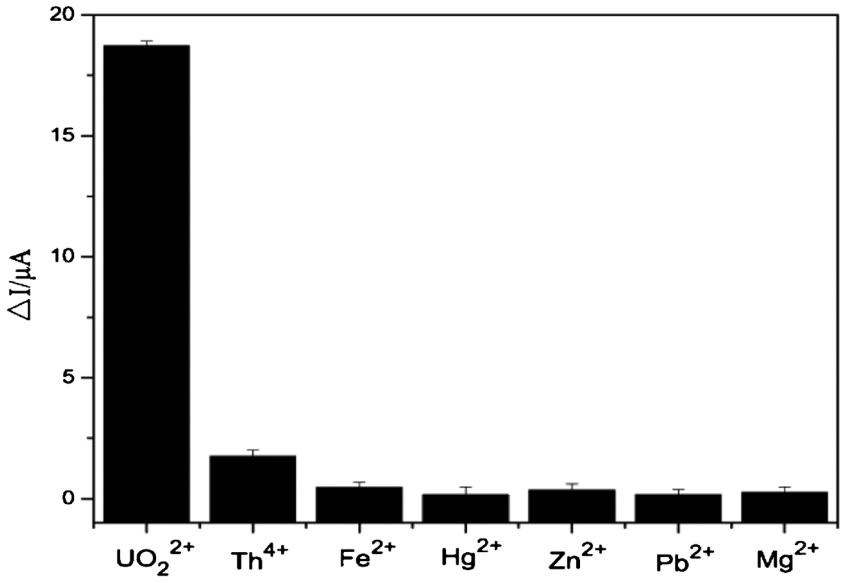

Fig. 7 DPV singles changed for sensors after reaction with various metal ions

Specificity of biosensors

In practical applications, the composition of the measured solution is more complex, and the biosensor sensitivity and selectivity requirements are higher, so the sensor in a complex environment of the selectivity is necessary. UO_2^{2+}, Th^{4+}, Fe^{2+}, Hg^{2+}, Zn^{2+}, Pb^{2+} and Mg^{2+} were added to the solution, respectively. The peak current I of the measuring sensor is compared by the relative intensity $\Delta I = (I\text{-}I_0)$ (I_0 represents the peak current of the biosensor when no metal ion is present in the test solution).

As shown in Fig. 7, DPV signals of the sensor slightly changed after adding the metal ions, namely, Th^{4+}, Fe^{2+}, Hg^{2+}, Zn^{2+}, Pb^{2+}, and Mg^{2+} at 2 nM concentrations compared with UO_2^{2+} at 0.2 nM. The results confirmed that the response of the sensor to UO_2^{2+} was unaffected by the presence of other metal ions. Therefore, the sensor system has good selectivity for UO_2^{2+} in solution. The reproducibility and stability of the DNA sensor is investigated by the change of the peak current after the reaction on the modified electrode prepared by the same method, and precision and accuracy of the sensor, seeing the Supporting Information.

Table 2 Analytical results for UO_2^{2+} in actual samples (n = 5) and recovery

Sample	Added/(pM)	Found/(pM)	Recovery/%	RSD/%
Lake water	30	27.4	91.3	3.4
	50	49.7	99.4	2.1
Tap water	30	28.6	95.3	4.5
	50	48.1	96.2	3.6

Vlake water = 20 mL,Vtap water =20 mL, Recovery = (Found /add) * 100

The actual sample detection

To investigate the validity of the procedure, the method was used to determine trace UO_2^{2+} in real sample by adding standard uranium solutions to lake water and tap water samples. The analytical results are listed in Table 2.

The results show that the sensor can detect trace UO_2^{2+} in aqueous solution, and the detection effect is excellent. From above results, it can be seen that the sensor can detect the trace amount of UO_2^{2+} in the aqueous solution, and the recovery rate is in the range of 91.3–99.4%.

Conclusions

In conclusion, an ultrasensitive electrochemical detection method for UO_2^{2+} based on specific DNAzyme and mesoSiNPs was designed. Results show that this strategy provides high selectivity and sensitivity for UO_2^{2+} detection. There exists a good linear correlation from 20 pM to 0.1 nM. The detection limit is 0.15 pM, which is lower than those of reported UO_2^{2+} detection methods. However, the analysis takes a few seconds than others due to the release of MB entrapped in the MSN process. Moreover, the assay was validated in real samples of spiked environmental water, and the results demonstrated its practical feasibility. Therefore, it is economical, effective, highly selective and practical. In view of these advantages, we deem that this assay will have some potential applications in environmental monitoring field.

Acknowledgements This research was supported by the National Natural Science Foundation of China (11405081), the Hunan Provincial Natural Science Foundation of China (2017JJ3276) and the Department of Education of Hunan Province (17B226).

Compliance with ethical standards The author(s) declare that they have no competing interests.

References

1. Liu JW, Brown AK, Meng X, Cropek DM, Istok JD, Watson DB, Lu Y (2007) A catalytic beacon sensor for uranium with parts-per-trillion sensitivity and millionfold selectivity. P Natl Acad Sci 104: 2056–2061. doi:10.1073/pnas.0607875104
2. Gongalsky KB (2003) Impact of pollution caused by uranium production on soil macrofauna. Environ Monit Asses 89:197–219. doi:10.1023/A:1026031224658
3. Villa M, Manjon G, Hurtado S, García-Tenorio R (2011) Uranium pollution inan estuary affected by pyrite acid mine drainage and releases of naturally occurring radioactive materials. Mar Pollut Bull 62:1521–1529. doi:10.1016/j.marpolbul.2011.04.003
4. Alam MN, Rahman N, Azmi SNH (2008) Optimized and validated spectrophotometric method for the determination of uranium(VI) via complexation with meloxicam. J Hazard Mater 155:261–268. doi:10.1016/j.jhazmat.2007.11.055
5. Xiao G, Jones RL, Saunders D, Caldwell KL (2014) Determination of 234U/238U, 235U/238U and 236U/238U isotope ratios in urine using sector field inductively coupled plasma mass spectrometry. Radiat Prot Dosim 1:1–7. doi:10.1093/rpd/ncu023
6. Santos JS, Teixeira Leonardo SG, Dos Santos Walter NL, Lemos VA, Godoy JM, Ferreira Sérgio LC (2010) Uranium determination using atomic spectrometric techniques:an overview. Anal Chim Acta 674:143–156. doi:10.1016/j.aca.2010.06.010
7. Michon J, Frelon S, Garnier C, Coppin F (2010) Determinations of uranium(VI) binding properties with some metalloproteins (transferrin, albumin, metallothionein and ferritin) by flluorescence quenching. J Fluoresc 20:581–590. doi:10.1007/s10895-009-0587-3
8. Dutta RK, Kumar A (2016) Highly sensitive and selective method for detecting ultratrace levels of aqueous uranyl ions by strongly photoluminescent-responsive amine-modified cadmium sulfide quantum dots. Anal Chem 88:9071–9078. doi:10.1021/acs.analchem. 6b01943
9. Zhang D, Chen Z, Omar H, Deng L, Khashab NM (2015) Colorimetric peroxidase mimetic assay for uranyl detection in sea water. ACS Appl Mater Interfaces 7:4589–4594. doi:10.1021/am507361x
10. Breaker RR, Joyce GF (1994) A DNA enzyme that cleaves RNA. Chem Biol 1:223–229. doi:10.1016/1074-5521(94)90014-0
11. Hu KC, Lan DX, Li XM, Zhang SS (2008) Electrochemical DNA biosensor based on nanoporous gold electrode and multifunctional encoded DNA-Au bio bar codes. Anal Chem 80:9124–9130. doi:10.1021/ac8017197
12. Viswanathan S, Radecka H, Radecki J (2009) Electrochemical biosensor for pesticides based on acetylcholinesterase immobilized on polyaniline deposited on vertically assembled carbon nanotubes wrapped with ssDNA. Biosens Bioelectron 24:2772–2777. doi:10.1016/j.bios.2009.01.044
13. Zhang J, Shi PW, Yan PP, Wang MB, Tang QH, Cai FD, Deng AP, Li JG (2015) Quantum dots based electrochemiluminescent immunosensor for ultrasensitive and specific determination of mercury (II) ions using gold nanoparticles and a monoclonal antibody. J Electrochem Soc 162:B22–B26. doi:10.1149/2.0631501jes
14. Lee JH, Wang Z, Liu J, Lu Y (2008) Highly sensitive and selective colorimetric sensors for uranyl (UO_2^{2+}):development and comparison of labeled and label-free DNAzyme -gold nanoparticle systems. J Am Chem Soc 130:14217–14226. doi:10.1021/ja803607z
15. Zhang HY, Ruan YJ, Lin L, Lin M, Zeng XX, Zeng X, Fu FF (2015) A turn-off fluorescent biosensor for the rapid and sensitive detection of uranyl ion based on molybdenum disulfide nanosheets and specific DNAzyme. Spectrochim Acta A 146:1–6. doi:10.1016/j.saa.2015.02.113
16. Baker SE, Cai W, Lasseter TL, Weidkamp KP, Hamers RJ (2002) Covalently bonded adducts of deoxyribonucleic acid (DNA) oligonucleotides with single-wall carbon nanotubes:synthesis and hybridization. Nano Lett 2:1413–1417. doi:10.1021/nl025729f
17. Zhang GY, Deng SY, Cai WR, Cosnier S, Zhang XJ, Shan D (2015) Magnetic zirconium hexacyanoferrate (II) nanoparticle as tracing tag for electrochemical DNA assay. Anal Chem 87:9093–9100. doi:10.1021/acs.analchem.5b02395
18. Ma DD, Yuan YL, Xiao XL, Gao YY, Li YH, Xu WH, Long W (2014) A label-free electrochemical biosensor for trace uranium based on DNAzymes and gold nanoparticles. J Radioanal Nucl Chem 299:1911–1919. doi:10.1007/s10967-013-2897-9
19. Tang Q, Yuan YL, Xiao XL, Guo P, Hu JB, Ma DD, Gao YY (2013) DNAzyme based electrochemical sensors for trace uranium. Microchim Acta 180:1059–1064. doi:10.1007/s00604-013-1021-8
20. Ren K, Wu J, Zhang Y, Yan F, Ju HX (2014) Proximity hybridization regulated DNA biogate for sensitive electrochemical immunoassay. Anal Chem 86:7494–7499. doi:10.1021/ac5012377
21. Qin QD, Ma J, Liu K (2009) Adsorption of anionic dyes on ammonium-functionalized MCM-41. J Hazard Mater 162:133–139. doi:10.1016/j.jhazmat.2008.05.016
22. Shao Y, Wang X, Kang Y, Shu Y, Sun Q, Li L (2014) Application of Mn/MCM-41 as an adsorbent to remove methyl blue from aqueous solution. J Colloid Interface Sci 429:25–33. doi:10.1016/j.jcis.2014.05.004
23. Xiao N, Deng J, Cheng JL, Ju SQ, Zhao HQ, Xie J, Qian D (2016) Carbon paste electrode modified with duplex molecularly imprinted polymer hybrid film for metronidazole detection. Biosens Bioelectron 81:54–60. doi:10.1016/j.bios.2016.02.041
24. van der Maaden K, Sliedregt K, Kros A, Jiskoot W, Bouwstra J (2012) Fluorescent nanoparticle adhesion assay:a novel method for surface pKa determination of self-assembled monolayers on silicon surfaces. Langmuir 28:3403–3411. doi:10.1021/la203560k
25. Vashist SK, Lam E, Hrapovic S, Male KB, Luong John HT (2014) Immobilization of antibodies and enzymes on 3-aminopropyltriethoxysilane-functionalized bioanalytical platforms for biosensors and diagnostics. Chem Rev 114:11083–11130. doi:10.1021/cr5000943
26. Gonza'lez AG, Herrador MA (2007) A practical guide to analytical method validation, including measurement uncertainty and accuracy profiles. Trac-Trend Anal Chem 26:227–238. doi:10.1016/j.trac.2007.01.009
27. Yun W, Cai D, Jiang J, Wang X, Liao JS, Zhang PC, Sang G (2016) An ultrasensitive electrochemical biosensor for uranyl detection based on DNAzyme and target-catalyzed hairpin assembly. Microchim Acta 183(4):1425–1432. doi:10.1007/s00604-016-1778-7
28. Zhou B, Wang YS, Yang HX, Xue JH, Wang JC, Liu SD, Zhao H (2014) A sensitive resonance light scattering assay for uranyl ion based on the conformational change of a nuclease-resistant aptamer and gold nanoparticles acting as signal reporters. Microchim Acta 181(11–12):1353–1360. doi:10.1007/s00604-014-1267-9